Observations

of the

CALIFORNIA INSTITUTE OF TECHNOLOGY

RADIO OBSERVATORY

Owens Valley, California

1961

5. BRIGHTNESS DISTRIBUTION IN DISCRETE RADIO SOURCES. II. OBSERVATIONS WITH A NORTH-SOUTH INTERFEROMETER

by

P. Maltby

BRIGHTNESS DISTRIBUTION IN DISCRETE RADIO SOURCES. II. OBSERVATIONS WITH A NORTH-SOUTH INTERFEROMETER

by

P. Maltby

California Institute of Technology
Radio Observatory

Owens Valley, California

ABSTRACT

Information about the brightness distribution in 165 radio sources has been obtained at a wavelength of 31.3 cm. The measurements were made with the variable spacing interferometer at the Owens Valley Radio Observatory using a north-south baseline. Primary sets of observations, giving the visibility amplitude and the phase, were taken at transit at four different antenna spacings. Additional information about the brightness distribution was obtained from observations at large hour angles, using the same physical antenna separations. The results of the observations are given in tabular form and several visibility curves are shown.

I. INTRODUCTION

During the winter of 1960-61, the brightness distributions in 165 radio sources were investigated, using a north-south baseline. Ninety-nine of the observed sources have also been investigated by Moffet (1962) using an east-west baseline. The sources were mainly selected from the third Cambridge survey (3C) by Edge, Shakeshaft, McAdam, Baldwin and Archer (1959), and the first Sydney survey by Mills, Slee and Hill (1958). In order to eliminate possible spurious effects caused by the sun, the observations

were taken mainly at night. Thus, only sources having right ascensions between 21^h and 16^h were observed. The sources which were selected have declinations between -45° and $+73^\circ$. All observations were taken at a wavelength of 31.3 cm.

II. APPARATUS

The interferometer consists of two equatorially mounted, 90-ft paraboloids. The antennas could be moved along railroad tracks to fixed observing stations. The available antenna separations in the north-south direction were 200 ft, 400 ft, 800 ft and 1600 ft when these observations were taken. A detailed description of the interferometer and its geometry is given elsewhere by Read (1961).

As few observations with a north-south interferometer have hitherto been reported, a brief discussion of the geometry of this configuration will be given here. Let the radio source make an angle θ with the plane normal to the line joining the two antennas. If the antenna separation measured in wavelengths is $\underline{s}$, the difference in path length between the signals received from the two antennas is $\underline{s} \sin \theta$. For a north-south interferometer with no azimuth or level errors, the angle θ may be written (see Moffet 1962),

$$\sin \theta = \sin \delta \cos \phi - \cos \delta \sin \phi \cos h, \tag{1}$$

where h and δ are the hour angle and the declination of the source, respectively, and ϕ is the latitude of the observatory site. In particular for observations at transit, equation (1) reduces to,

$$\theta = \delta - \phi .$$

The effective antenna separation of a north-south interferometer is equal to $\underline{s} \cos \theta$, where θ is given by equation (1). For observations at transit, the effective antenna separation depends on the declination of the source, contrary to the situation with an east-west interferometer. One also has to consider the fact that sources far from the zenith are difficult to observe with a north-south interferometer, because one antenna may shadow the other in the direction of the source. In our case, sources with declination less than -25° could not be observed at transit at the 200-ft station, while sources with declination higher than -45° could be observed at the maximum antenna separation.

The position angle, $\underline{p}$, (measured positive from north towards east), at which the source is observed with a north-south interferometer is given by

$$\tan \underline{p} = - \frac{\sin \phi \sin h}{\cos \phi \cos \delta + \sin \phi \sin \delta \cos h} . \tag{2}$$

For observations at transit with a north-south interferometer, the position

angle is equal to zero. At other hour angles it is possible to observe the source in other position angles.

For a north-south interferometer the source is moving parallel to the interferometer fringes when the source is at the meridian. A lobe rotator was therefore used to rotate the phase of the local oscillator signal sent to the mixer in one of the antennas. The amount of phase rotation, η, was indicated on the receiver chart by marks placed each time the phase had the same value. The apparent declination is determined by,

$$\frac{N\pi+\eta}{s} + \Delta t = \sin\delta \cos\phi - \cos\delta \sin\phi \cos h, \qquad (3)$$

where N is an integer chosen from an approximate knowledge of the source position and Δt is determined by the instrumental phase error, which may change through the night. The change of Δt may be found from observations of sources with known positions. The determination of the phase consists of comparing the apparent declination of the source at different antenna separations.

For a north-south interferometer the path lengths traversed by the signals from the antennas are different even at transit. The path lengths were equalized by adjusting a variable delay line. The change in gain due to the variable attenuation of the delay line was compensated, and the accuracy in this adjustment was better than 1 %.

III. THE OBSERVATIONS

In order to determine the brightness distribution, it is necessary to know the relative source intensity as well as the phase at each antenna separation. The amplitude and the phase determine the complex visibility function which is related to the brightness distribution by a Fourier transformation (see e.g. Moffet 1962).

The main problem in the measurement of the amplitude and phase is the correction for instrumental changes. Slight variations in the performance of the equipment are to be expected in the course of a night, from night to night and at different antenna separations. These changes can be allowed for by observing several sources of angular extent small compared with the resolution of the interferometer. For a small diameter source, the visibility amplitude may be regarded as independent of antenna separation. Morris, Palmer and Thompson (1957) reported three sources, 3C 147, 3C 196 and 3C 295, with angular extent less than 12". In addition, 3C 123 and 3C 48 were found by Moffet (1962) to have small diameters. As these sources have only been observed in the east-west direction, they do not necessarily show a small diameter in the north-south direction. In fact, 3C 123 was found to have a diameter of 30" in the north-south direction. In the following we have assumed that the other four sources listed above have small angular extent, and we have used them as calibrators of amplitude. In addition to these small diameter sources, several sources with relatively high intensity were used as amplitude calibrators while at any one observing station. During the whole observation period the gain stability was found to be good; the uncertainty in the amplitude calibration was less than 3 %.

Primary sets of observations were made at transit with horizontal antenna separations of 195, 389, 779 and 1557 wavelengths. Also, measurements by Harris and Roberts (1960) with a single antenna at the same wavelength were available. The relative intensity of each source observed at transit is given in Table 1, together with the value of cos θ, which is the conversion factor between the effective and the actual antenna separation.

No individual values for the accuracy of the observations are given in Table 1, for the following reason. Except in a very few cases, each relative intensity in Table 1 is based on three observations. The r.m.s. error based on only three observations may be somewhat misleading. Therefore, the error in each relative intensity may be taken as the mean of the r.m.s. errors for all sources with the same intensity. In Figure 1 the mean of the r.m.s. errors, $\overline{\sigma}$, in percentage of the intensity of the source, is plotted against the source intensity. This curve may be used to estimate the accuracy of each relative intensity in Table 1. We see from Figure 1 that the uncertainty is approximately inversely proportional to the intensity of the source. It would appear that for most of the observed sources the uncertainty is caused by receiver noise and not by gain variations.

The observations of faint radio sources are limited by the angular resolution of each of the antennas. The magnitude of this confusion problem for the present observations may be estimated by computing the probability of having more than one source in the primary beam simultaneously. In this case the primary beam is 0.5 square degree and the intensity of the weakest source observed is 1.8×10^{-26} W $m^{-2}(c/s)^{-1}$. Errors in the visibility curve resulting from confusion may amount to 10% for about the fifteen weakest sources.

Another possible source of error is the effect of not pointing the antennas precisely in the direction of the source. This will not influence the visibility curve if the source is still within the primary beam of the individual antennas, and if the same pointing error was present at all antenna separations. The estimated intensity of the source will, nevertheless, be in error. Adequate care was taken in the directing of the antennas, and the number of cases where the pointing error is significant is certainly very small.

Table 1 also gives the intensity of each source. The intensity was obtained from an extrapolation of the visibility curve to an antenna separation equal to zero. For sources also observed in the east-west direction by Moffet (1962), the intensity was deduced from a comparison of both visibility curves. In those cases where the source was observed by Harris and Roberts (1960) with a single antenna, their intensity value was taken into account. The source intensities are corrected for extinction, and the strongest sources are corrected for the deviation from linearity of the detector law. The source Virgo A was used as a standard source, with an assumed flux density of 300×10^{-26}W $m^{-2}(c/s)^{-1}$ at a wavelength of 31.3 cm.

In Table 2 is given the relative phase as compared with the phase observed at a physical antenna separation of 200 ft. The phase was deduced after the relative intensities were obtained. Thus several sources showing little or no change in intensity as a function of antenna separation could be used as phase calibrators. Only those sources are listed for which the change in phase differs significantly from zero. In Table 2 a positive phase represents as apparent shift of the position towards north with increasing antenna spacing.

The phase measurements were sometimes not as accurate as desirable. However, the phase information was very useful as a check on the interpretation of the visibility curves.

A second set of observations was taken at other hour angles, in order to obtain information about the visibility curves in other position angles. No attempt was made to recover the phase information in these off-transit observations. The source was observed at the same hour angle at each antenna spacing in order to maintain the same orientation at the different antenna separations. The off-transit observations were made for a selected number of sources at all spacings except the closest one. The observations were taken at, or close to, position angles 30° and 150°. The results are given in Tables 3 and 4, together with cos θ, the conversion factor between the effective and the horizontal antenna spacing. The position angle in which the source was observed is also given in Tables 3 and 4. Each value in these tables is usually based on two observations. Figure 1 cannot, therefore, be used to determine the r.m.s. error. The estimated uncertainty is given in the tables.

IV. CONCLUDING REMARKS

From the amplitude and the phase information we obtain the complex visibility curve. Using the data given in Table 1, we can plot the relative intensity against the effective antenna separation; the visibility curve. In Figures 2 to 6 the visibility curve V(s) is shown for several sources with components larger than about 1.5. Unless otherwise noted, the observations refer to position angle zero.

In Figures 2 to 6 we find a large number of cases where a high second maximum is present in the visibility curve of the source. A high second maximum is usually associated with a change in the apparent position of the source (Table 2). It can be shown that the highest second maximum in the visibility curve for a symmetrical source is obtained by a source with uniform brightness across the source. By comparing the visibility curves with those corresponding to a source with uniform brightness, we find that several of the sources are asymmetrical. In many cases it is necessary to assume that the source consists of two well-spaced components in order to explain the observations.

The program of research in radio astronomy at the California Institute of Technology is supported by the United States Office of Naval Research under Contract Nonr 220(19). The author wishes to thank G. J. Stanley, Acting Director of the Observatory, and A. T. Moffet for helpful discussions, and several colleagues for their assistance in the observational program. The author is a recipient of a Fulbright Travel Grant and a grant from the Norwegian Research Council for Science and the Humanities.

REFERENCES

Edge, D. O., Shakeshaft, J. R., McAdam, W. B., Baldwin, J. E. and Archer, S. 1959, Memoirs Roy. Astr. Soc., 68, 37.

Harris, D. E. and Roberts, J. A. 1960, Pub. A. S. P., 72, 237.

Mills, B. Y., Slee, O. B. and Hill, E. R. 1958, Aust. J. Phys., 11, 360.

Moffet, A. T. 1962, Ap. J., (submitted).

Morris, D., Palmer, H. P. and Thompson, A. R. 1957, The Observatory, 77, 103.

Read, R. B. 1961, Trans. I.R.E., AP-9, 31.

Wilson, R. W. and Bolton, J. G. 1960, Pub. A. S. P., 72, 331.

LEGENDS FOR FIGURES

Figure 1 - The mean of the r.m.s. errors, $\overline{\sigma}$, in percentage of the intensity of the source plotted against the source intensity.

Figure 2-6 - The visibility amplitude $V(\underline{s})$ is plotted against the antenna spacing $\underline{s}$ for selected sources. Unless otherwise noted, the observations refer to position angle zero.

TABLE I

FLUXES AND VISIBILITY AMPLITUDES FOR TRANSIT OBSERVATIONS

Source	Flux	cos θ	Spacing/cos θ				
			0	195λ	389λ	779λ	1557λ
CTA 1	(13.0±1.5)*	0.820	1.00±.12	0.27	0.13	0.05	0.05
3C 2	5.1±0.4	0.792	---	1.02	1.06	0.94	0.96
3C 5	2.3±0.5	0.902	---	---	1.07	0.80	0.84
MSH 00-29	4.0±0.6	0.410	---	---	1.00	0.97	1.06
S.N. 1572	(57.0±3.0)	0.894	1.00±.05	0.78	0.32	0.23	0.04
3C 15	5.5±0.4	0.781	0.93±.21	0.98	1.03	0.99	0.96
3C 17	7.8±0.5	0.769	1.30±.30	0.99	1.00	0.94	0.94
3C 18	5.9±0.3	0.887	---	0.99	0.94	0.81	0.56
3C 19	4.5±0.8	0.997	---	0.85	1.00	0.98	0.96
3C 20	14.7±1.8	0.968	0.93±.11	1.08	1.00	0.99	1.01
MSH 00-222	9.3±0.9	0.456	---	0.89	0.71	0.52	0.41
3C 23	2.8±0.7	0.941	---	0.79	0.99	0.67	0.88
CTA 6	(15.6±1.2)*	0.944	1.00±.08	0.20	<0.09	<0.04	<0.04
3C 26	3.2±0.6	0.755	---	1.21	0.95	0.90	1.01
3C 27	10.3±1.5	0.858	1.05±.15	0.93	0.90	0.98	0.85
3C 28	2.7±0.3	0.981	0.89±.33	0.99	1.01	0.87	0.90
3C 29	9.2±0.9	0.778	---	0.92	0.74	0.62	0.31
3C 32	6.0±0.6	0.594	1.20±.25	1.01	0.95	0.93	0.90
3C 33	18.6±0.9	0.912	0.97±.03	0.94	0.60	0.61	0.36
3C 38	7.0±0.7	0.602	1.19±.22	0.96	0.82	0.82	0.92
3C 40	8.0±1.2	0.779	1.00±.22	0.60	0.39	0.38	0.12
3C 41	(6.9±0.9)	0.997	1.00±.13	0.62	0.71	0.48	0.58
3C 43	3.9±0.4	0.970	---	0.98	0.93	0.92	0.97
3C 46	1.9±0.4	1.000	---	1.03	0.88	0.78	0.55
3C 47	6.2±0.5	0.959	1.01±.15	0.98	0.95	0.75	0.34
3C 48	21.5±1.1	0.997	0.98±.08	Standard source			
3C 55	4.5±0.7	0.988	---	0.98	0.79	0.91	0.77
MSH 01-315	5.2±0.5	0.368	---	---	0.98	1.01	0.94
3C 58	35.0±2.4	0.888	0.95±.05	0.98	0.82	0.49	0.08
3C 62	7.0±0.7	0.635	---	0.72	1.00	0.94	0.94
3C 63	5.3±0.8	0.773	1.15±.19	0.93	1.04	0.95	0.86
3C 65	5.0±1.0	0.999	---	0.86	0.91	1.00	0.86
3C 66	(12.9±0.9)	0.995	1.00±.08	0.86	0.54	0.31	0.28
3C 69	5.3±0.5	0.929	---	0.99	0.95	0.84	0.66
MSH 02-110	6.4±0.4	0.546	---	1.01	0.99	0.94	1.03
3C 71	6.9±0.3	0.794	---	1.00	1.01	1.00	0.97
3C 75	8.1±0.4	0.854	0.92±.08	0.96	0.73	0.29	0.20
3C 78	9.1±1.4	0.837	---	1.05	1.11	0.96	0.67
3C 79	7.0±0.5	0.938	0.97±.08	1.04	0.99	0.90	0.95
CTA 21	9.3±0.7	0.934	0.97±.11	1.05	1.00	0.96	0.98

TABLE 1 -continued

Source	Flux	cos θ	Spacing/cos θ				
			0	195λ	389λ	779λ	1557λ
NGC 1275	20.4±2.1	0.997	1.05±.11	0.86	0.76	0.71	0.57
Fornax A	(125.0±6.0)*	0.266	1.00±.04	---	0.39	0.05	0.01
3C 86	(12.1±0.9)	0.951	1.00±.08	0.81	0.75	0.58	0.94
3C 88	6.9±0.5	0.820	---	0.96	0.90	0.68	0.25
3C 89	(6.3±0.9)	0.781	1.00±.16	0.65	0.71	0.63	0.41
CTA 26	2.8±0.4	0.776	1.25±.41	0.97	0.90	0.57	0.81
MSH 03-19	4.9±0.5	0.618	---	0.95	0.83	0.71	0.34
MSH 03-2I2	8.1±0.8	0.420	---	---	0.92	0.68	0.39
3C 98	(14.1±1.2)	0.891	1.00±.08	0.96	0.63	0.34	0.20
3C 103	7.2±0.5	0.995	0.92±.08	1.00	0.87	0.62	0.27
3C 105	7.5±0.8	0.833	---	0.95	0.78	0.53	0.50
MSH 04-12	4.2±0.3	0.647	---	0.98	1.01	0.95	0.83
3C 109	5.9±0.6	0.898	0.86±.16	1.04	0.98	0.84	0.35
MSH 04-24	4.2±0.4	0.525	---	0.95	1.00	0.85	0.76
3C 111	(20.4±2.0)	1.000	1.00±.08	0.97	0.89	0.58	0.14
3C 119	9.8±0.7	0.997	---	0.98	0.97	1.00	0.94
MSH 04-112	3.2±0.6	0.634	---	---	0.91	0.68	<0.06
3C 123	64.3±1.9	0.991	1.00±.03	1.00	1.01	0.98	0.88
MSH 04-218	10.4±0.5	0.414	---	---	1.00	0.94	0.77
3C 129	10.6±1.1	0.991	0.89±.11	1.00	0.73	0.36	0.23
3C 131	4.5±0.7	0.995	---	0.93	1.00	0.84	0.92
3C 132	5.9±1.5	0.969	---	0.94	0.77	0.74	0.71
3C 133	8.4±1.7	0.979	---	0.68	0.97	0.88	0.80
3C 134	15.1±0.8	1.000	1.00±.08	0.93	0.76	0.24	0.45
MSH 05-13	1.8±0.5	0.560	---	0.83	0.96	0.80	0.89
3C 135	2.9±0.3	0.806	---	1.01	0.94	0.69	0.69
Pictor A	(86.8±2.6)	0.121	1.01±.07	---	---	0.98	0.99
3C 138	11.9±0.7	0.936	---	0.99	1.01	0.99	0.93
MSH 05-36	21.2±1.0	0.272	---	---	1.00	0.94	0.95
3C 141	3.7±0.6	0.997	---	0.97	0.89	0.83	0.63
Crab Neb.	(1030±45)	0.965	1.00±.04	0.88	0.68	0.19	0.06
Orion Neb.	(361±9)	0.736	1.00±.03	0.75	0.46	0.14	0.01
3C 147	29.2±0.9	0.976	0.99±.03	Standard source			
3C 153	6.3±0.6	0.982	---	0.96	0.94	1.00	0.93
3C 154	7.2±0.5	0.981	0.95±.08	1.00	1.04	1.00	0.97
1C 443	(129±6)*	0.968	1.00±.05	0.07	0.02	0.01	0.01
3C 158	3.5±0.4	0.922	---	0.98	1.00	0.96	0.90
3C 159	4.1±0.5	0.999	---	1.00	0.98	0.92	0.75
3C 161	25.6±1.3	0.730	0.93±.06	1.00	0.98	0.93	0.90
Rosette Neb.	(105±2)*	0.845	1.00±.02	0.04	0.01	0.01	<0.01
3C 166	3.8±0.3	0.962	---	0.99	0.97	0.84	0.80
3C 171	5.7±0.4	0.956	1.05±.16	0.98	1.01	0.95	0.88
MSH 06-216	5.1±0.4	0.478	---	0.96	1.00	0.95	1.01

TABLE 1 -continued

Source	Flux	cos θ	Spacing/cos θ				
			0	195λ	389λ	779λ	1557λ
3C 172	4.9±0.7	0.979	---	0.95	0.78	0.53	0.32
3C 175	4.1±0.4	0.904	---	1.13	0.95	1.00	0.89
3C 178	2.3±0.5	0.682	---	1.00	0.85	0.93	1.01
3C 180	4.3±0.6	0.775	---	1.02	0.85	0.72	0.23
3C 184	2.7±0.5	0.838	---	0.96	1.00	1.00	0.92
3C 187	2.7±0.5	0.818	---	1.00	0.85	0.45	0.63
MSH 07-117	4.0±0.8	0.556	---	0.88	0.81	0.62	0.98
3C 191	2.9±0.4	0.892	---	1.00	1.03	0.98	1.00
3C 192	7.4±0.5	0.974	---	0.97	0.93	0.69	0.16
3C 195	5.5±0.7	0.674	---	1.00	0.91	0.89	0.39
3C 196	20.4±0.8	0.981	1.03±.07	Standard source			
3C 198	3.4±0.3	0.855	---	0.92	0.64	0.37	<0.24
Puppis A	(105±6)*	0.172	1.00±.06	---	0.17	0.07	0.02
3C 202	3.9±0.5	0.939	---	0.95	1.00	0.83	0.59
3C 208	4.9±1.2	0.919	---	0.67	0.60	0.83	0.65
3C 212	3.8±0.6	0.922	---	1.01	0.90	1.02	0.94
MSH 08-219	8.2±0.6	0.453	---	0.96	0.99	1.00	0.98
3C 216	6.0±0.4	0.995	---	0.97	0.91	1.00	0.84
Hydra A	(67.5±1.8)	0.654	1.00±.03	0.93	0.88	0.76	0.64
3C 219	12.3±0.9	0.989	---	0.97	0.80	0.42	0.37
3C 225	4.8±1.0	0.919	---	0.97	0.79	0.98	0.51
3C 227	11.2±1.1	0.870	0.91±.09	1.00	0.86	0.83	0.77
3C 228	5.2±0.5	0.922	---	0.99	0.94	0.87	0.68
3C 230	5.9±0.4	0.798	---	0.99	1.01	0.86	0.70
3C 234	8.3±0.8	0.990	0.88±.12	0.94	0.95	0.81	0.73
3C 237	9.6±0.7	0.870	0.57±.10	0.98	1.01	0.89	0.86
3C 238	5.5±0.6	0.860	---	1.00	0.50	0.75	0.77
MSH 10-44	6.7±0.6	0.196	---	---	---	1.02	0.91
3C 243	2.1±0.5	0.861	---	1.10	0.82	0.55	0.86
3C 245	4.9±0.6	0.905	---	1.05	0.93	0.90	0.98
3C 254	5.1±0.4	0.998	---	1.00	0.90	0.92	0.96
MSH 11-18	6.6±1.0	0.630	---	0.81	1.00	0.90	1.00
3C 261	2.0±0.5	0.991	---	1.11	0.92	0.94	0.95
3C 264	(10.5±3.0)	0.955	1.00±.29	0.75	0.58	0.43	0.30
3C 265	4.8±0.5	0.994	---	0.90	1.02	0.89	0.86
3C 267	3.8±0.8	0.912	---	0.86	1.05	0.87	0.89
3C 270	(28.5±1.5)	0.856	1.00±.05	0.84	0.79	0.57	0.22
3C 273	45.4±1.4	0.820	1.11±.05	1.01	1.00	0.96	0.97
M 84	8.0±2.0	0.912	---	---	0.88	0.68	0.14
M 87	300	0.909	1.00±.05	0.78	0.57	0.60	0.52
3C 275	4.9±0.7	0.745	---	0.90	1.00	1.00	0.96
Coma A	4.0±0.6	0.986	---	1.07	0.97	0.97	0.95

TABLE 1 —concluded

Source	Flux	cos θ	Spacing/cos θ				
			0	195λ	389λ	779λ	1557λ
3C 278	10.6±1.1	0.649	0.91±.15	0.92	0.98	0.76	0.46
3C 279	9.8±0.7	0.733	0.70±.12	1.00	0.97	0.99	0.97
3C 280	7.2±0.7	0.983	0.95±.16	1.02	0.99	0.94	1.02
3C 283	8.6±0.9	0.510	1.18±.18	0.88	0.99	0.93	1.00
3C 286	19.8±1.4	0.994	0.99±.08	0.96	0.95	0.91	0.90
3C 287	9.4±0.9	0.979	0.90±.13	1.00	1.00	0.99	0.93
MSH 13-33	6.9±0.7	0.327	---	---	0.95	0.61	0.44
MSH 13-011	4.6±0.7	0.424	---	0.91	1.03	0.92	0.91
3C 295	32.0±1.0	0.965	0.95±.07	Standard source			
3C 298	9.7±0.5	0.861	1.15±.16	1.00	0.99	0.96	0.96
MSH 14-011	4.8±1.0	0.782	---	0.64	0.93	0.86	0.84
MSH 14+010	3.4±0.7	0.833	---	0.77	0.53	0.95	0.91
MSH 14-121	5.6±0.6	0.666	---	1.00	0.93	0.91	0.83
3C 310	12.7±0.9	0.982	0.85±.14	0.87	0.61	0.14	0.09
3C 313	6.0±0.9	0.873	0.91±.16	0.97	0.88	0.72	0.33
3C 315	6.1±0.6	0.982	1.00±.16	0.96	0.90	0.70	0.20
3C 317	10.0±0.7	0.866	1.00±.10	0.97	0.95	0.92	0.80
3C 318	4.1±0.6	0.957	0.72±.24	1.07	1.00	0.94	0.99
3C 324	4.2±0.6	0.963	1.50±.37	1.11	0.92	0.91	0.89
3C 327	12.3±1.2	0.817	0.95±.17	1.00	0.99	0.90	0.82
MSH 16+02	6.5±1.0	0.811	---	0.89	0.97	0.88	1.09
Herc. A	73.5±3.7	0.845	1.00±.08	---	---	0.86	---
Sagr. A	(700±140)*	0.405	1.00±.20	---	0.29	0.26	0.09
Cygnus A	(2160±120)	0.998	1.00±.06	1.00	0.95	0.95	0.64
3C 433	17.4±0.9	0.977	0.89±.09	1.00	0.96	0.91	0.84
3C 436	6.3±0.6	0.987	1.00±.12	0.76	0.72	0.53	0.26
3C 438	10.6±0.5	1.000	1.00±.06	1.00	0.96	0.95	0.91
3C 441	4.1±0.5	0.990	---	1.00	0.95	0.89	0.70
3C 442	4.6±0.5	0.916	---	0.99	0.91	0.25	<0.17
3C 444	13.6±0.7	0.581	1.00±.04	1.01	0.91	0.85	0.45
3C 445	(8.2±1.2)	0.770	1.00±.14	0.76	0.18	0.13	0.32
3C 446	(7.8±0.9)	0.737	1.00±.12	0.86	0.97	0.82	0.93
CTA 102	7.8±0.5	0.901	0.93±.08	1.01	0.97	0.98	0.93
3C 452	15.3±1.5	0.999	0.91±.06	1.01	0.93	0.78	0.45
3C 456	3.4±0.9	0.883	---	0.99	0.99	0.66	0.92
3C 459	(7.2±0.6)	0.835	1.00±.08	0.93	0.91	0.78	0.87
Cass. A	(3120±150)	0.932	1.00±.05	0.89	0.70	0.20	0.12
MSH 23-112	3.2±0.5	0.647	---	1.04	0.96	0.81	0.97
3C 465	(11.7±0.9)	0.983	1.00±.08	0.79	0.41	0.30	0.23
3C 469	2.3±0.6	0.997	---	0.96	1.00	0.76	0.58

Notes: All fluxes given in units of 10^{-26} $wm^{-2}(c/s)^{-1}$.
* Peak apparent flux from Harris and Roberts (1960) or Wilson and Bolton (1960).
( ) Flux from Harris and Roberts (1960) or Wilson and Bolton (1960).

TABLE 2

VISIBILITY PHASES FOR TRANSIT OBSERVATIONS*

Source	cos θ	Spacing/cos θ		
		389λ	779λ	1557λ
S.N. 1572	0.894	$2^{o} \pm 10^{o}$	$162^{o} \pm 30^{o}$	$315^{o} \pm 50^{o}$
3C 33	0.912	5 ± 25	- 55 ± 30	-100 ± 60
3C 40	0.779	-30 ± 20	- 92 ± 30	-174 ± 40
3C 41	0.997	23 ± 20	31 ± 40	106 ± 60
3C 58	0.888	10 ± 20	- 54 ± 30	- 10 ± 50
3C 66	0.995	14 ± 20	- 97 ± 30	38 ± 60
3C 75	0.854	- 1 ± 20	- 47 ± 30	-159 ± 60
3C 86	0.951	-40 ± 30	- 66 ± 40	-114 ± 60
3C 89	0.781	27 ± 20	44 ± 30	78 ± 60
CTA 26	0.776	----	- 52 ± 30	-102 ± 60
3C 98	0.891	14 ± 20	139 ± 30	197 ± 50
3C 103	0.995	-16 ± 20	- 17 ± 30	-144 ± 60
3C 111	1.000	- 8 ± 15	- 15 ± 25	120 ± 60
3C 129	0.991	-13 ± 15	2 ± 25	-105 ± 50
3C 134	1.000	-12 ± 15	0 ± 25	-164 ± 50
3C 135	0.806	12 ± 20	70 ± 30	122 ± 50
Crab Neb.	0.965	2 ± 15	7 ± 25	-154 ± 40
Orion Neb.	0.736	30 ± 15	67 ± 25	276 ± 50
3C 172	0.979	-18 ± 20	- 11 ± 30	160 ± 60
3C 187	0.818	0 ± 15	- 30 ± 30	-106 ± 50
MSH 07-117	0.556	82 ± 20	118 ± 40	350 ± 80
3C 208	0.919	51 ± 15	108 ± 30	260 ± 60
Hydra A	0.654	13 ± 15	44 ± 25	96 ± 40
3C 219	0.989	- 6 ± 20	5 ± 25	160 ± 40
3C 225	0.919	-45 ± 20	- 10 ± 40	-150 ± 60
3C 243	0.861	5 ± 20	35 ± 40	130 ± 60
MSH 13-33	0.327	----	- 27 ± 40	-121 ± 80
MSH 14+010	0.833	----	- 90 ± 40	-180 ± 80
3C 310	0.982	10 ± 20	- 39 ± 40	-143 ± 80
3C 445	0.770	0 ± 25	- 40 ± 25	-215 ± 80
Cass. A	0.932	2 ± 20	- 25 ± 30	-160 ± 40

* Only those sources are listed which have phases differing significantly from zero.

TABLE 3

VISIBILITY AMPLITUDES FOR OBSERVATIONS WITH RESOLUTION IN POSITION ANGLE ≈ 30°

Source	p°	cos θ	Spacing/cos θ		
			389λ	779λ	1557λ
MSH 00-222	33	0.59	0.50 ± .05	----	----
3C 38	31	0.75	0.85 ± .08	----	----
MSH 01-315	34	0.49	0.89 ± .11	----	----
3C 62	30	0.78	0.97 ± .05	----	----
3C 75	30	0.96	0.76 ± .05	----	----
Fornax A	36	0.35	0.08 ± .03*	----	----
3C 89	30	0.91	0.58 ± .10	----	----
3C 98	30	0.98	0.38 ± .04	----	----
3C 105	30	0.95	0.79 ± .10	----	----
MSH 04-218	33	0.54	0.99 ± .05	0.95 ± .05	----
3C 135	30	0.92	0.60 ± .10	0.63 ± .10	----
Pictor A	40	0.24	0.83 ± .03	----	----
MSH 05-36	36	0.38	0.93 ± .05	0.99 ± .05	----
Orion Neb.	30	0.87	0.45 ± .01	0.06 ± .01	0.01 ± .01
3C 175	30	0.99	0.89 ± .10	0.74 ± .10	----
3C 198	30	0.96	0.53 ± .10	<0.20	----
Puppis A	38	0.28	0.14 ± .01*	0.04 ± .01	0.04 ± .01
Hydra A	30	0.80	0.83 ± .02	0.67 ± .02	0.46 ± .02
3C 227	30	0.97	0.79 ± .05	0.42 ± .05	----
MSH 10-44	38	0.27	1.03 ± .08	0.97 ± .08	----
3C 270	30	0.96	0.50 ± .02	0.10 ± .02	<0.03
M 87	31	0.99	0.53 ± .01	0.52 ± .01	0.50 ± .01
3C 278	31	0.79	0.89 ± .04	0.65 ± .04	0.17 ± .04
MSH 14+010	30	0.95	0.78 ± .10	0.89 ± .15	0.69 ± .15
3C 313	30	0.97	0.81 ± .07	0.40 ± .07	0.58 ± .07
3C 327	30	0.94	0.88 ± .03	----	0.32 ± .04

* Intensity is changing relatively quickly with time.

TABLE 4

VISIBILITY AMPLITUDES FOR OBSERVATIONS WITH RESOLUTION IN POSITION ANGLE ≈ 150°

Source	p°	cos θ	Spacing/cos θ		
			389λ	779λ	1557λ
3C 15	150	0.91	1.04 ± .05	0.81 ± .10	0.82 ± .10
3C 17	150	0.90	1.04 ± .05	0.82 ± .07	0.62 ± .07
MSH 00-222	147	0.59	0.67 ± .04	0.55 ± .05	----
3C 29	150	0.91	0.69 ± .05	0.56 ± .05	<0.12
3C 33	150	0.99	0.80 ± .03	0.45 ± .03	----
3C 38	149	0.75	0.75 ± .07	0.89 ± .07	0.73 ± .08
3C 40	150	0.91	----	0.32 ± .07	----
MSH 01-315	146	0.49	1.01 ± .05	1.00 ± .07	----
3C 62	150	0.78	0.99 ± .05	0.61 ± .05	0.61 ± .06
3C 75	150	0.96	0.75 ± .05	0.31 ± .05	0.28 ± .05
Fornax A	144	0.35	0.32 ± .03	----	----
3C 89	150	0.91	0.60 ± .10	0.50 ± .10	----
3C 98	150	0.98	0.82 ± .03	0.28 ± .05	0.48 ± .04
3C 105	150	0.95	0.64 ± .05	0.66 ± .05	0.55 ± .05
MSH 04-218	147	0.54	0.99 ± .05	0.87 ± .08	0.60 ± .06
3C 135	150	0.92	0.59 ± .10	0.56 ± .10	0.57 ± .10
Pictor A	140	0.24	0.84 ± .03	0.84 ± .03	----
MSH 05-36	144	0.38	0.99 ± .03	0.95 ± .05	----
Orion Neb.	150	0.87	0.37 ± .01	0.12 ± .01	0.04 ± .01
3C 175	150	0.99	0.91 ± .10	0.95 ± .10	0.87 ± .10
3C 198	150	0.96	0.69 ± .10	0.33 ± .10	----
Puppis A	142	0.28	0.21 ± .01	0.02 ± .01*	0.02 ± .01*
Hydra A	150	0.80	0.89 ± .02	0.81 ± .02	0.77 ± .02
3C 227	150	0.97	0.87 ± .05	0.50 ± .05	0.17 ± .05
MSH 10-44	142	0.27	----	0.89 ± .07	0.63 ± .07
3C 270	150	0.96	----	0.09 ± .02	0.06 ± .02
M 87	149	0.99	----	0.52 ± .01	----
3C 278	149	0.79	----	0.66 ± .05	0.28 ± .05
3C 445	150	0.90	0.15 ± .05	0.22 ± .05	----
3C 446	150	0.87	0.97 ± .05	0.98 ± .05	----

* Intensity is changing relatively quickly with time.

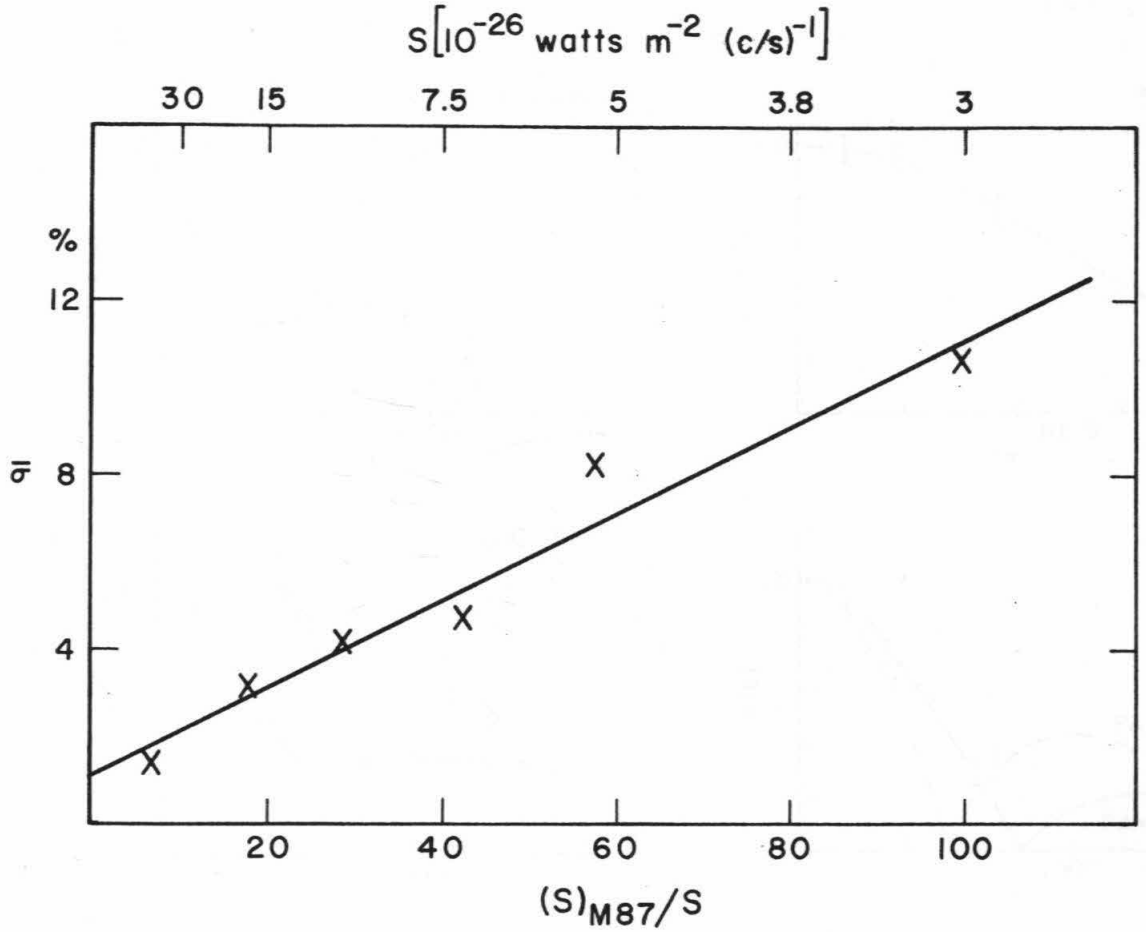

FIGURE 1

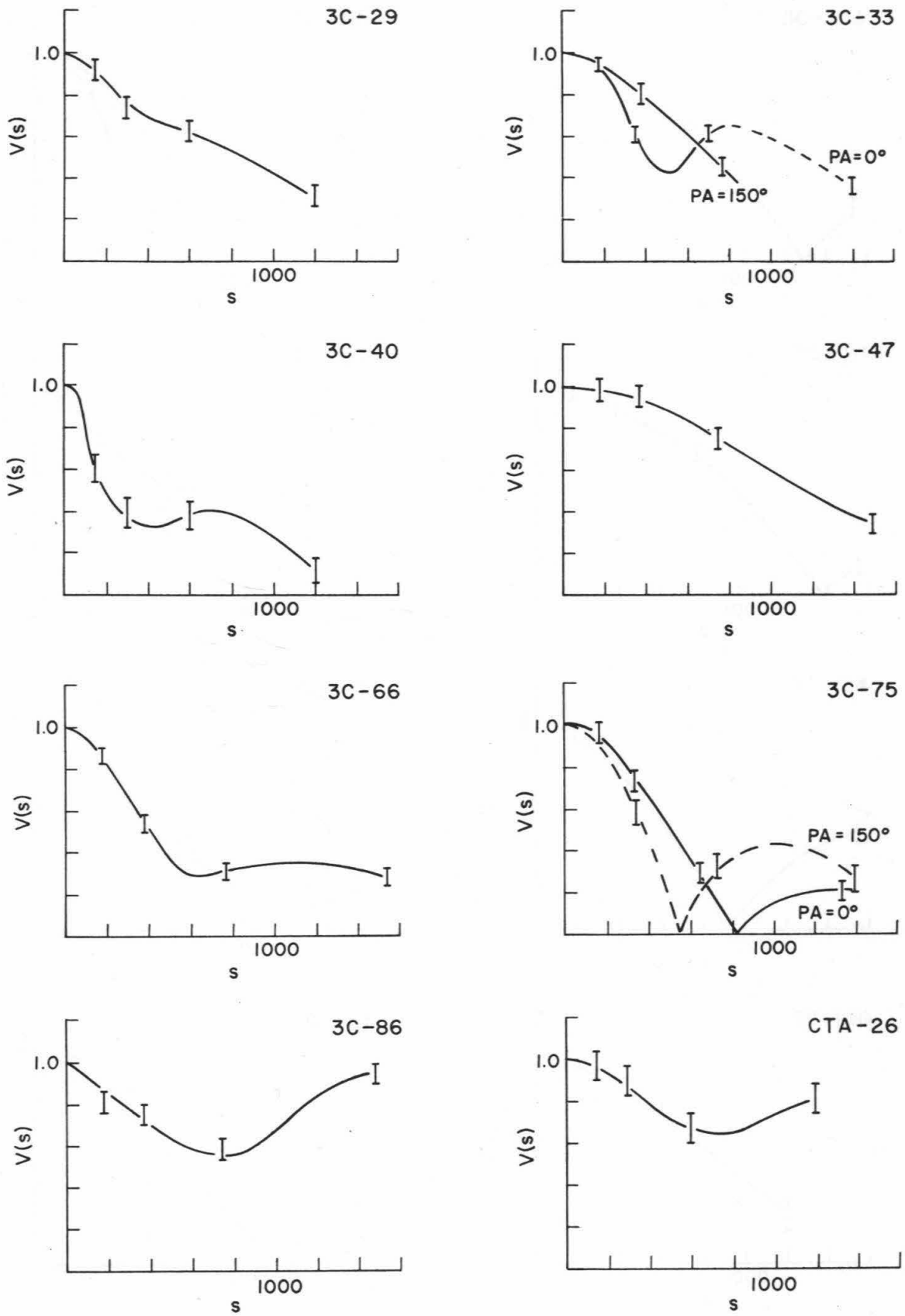
3C-29
1.0
V(s)
1000
s
3C-33
1.0
V(s)
PA=0°
PA=150°
1000
s
3C-40
1.0
V(s)
1000
s
3C-47
1.0
V(s)
1000
s
3C-66
1.0
V(s)
1000
s
3C-75
1.0
V(s)
PA=150°
PA=0°
1000
s
3C-86
1.0
V(s)
1000
s
CTA-26
1.0
V(s)
1000
s

FIGURE 2

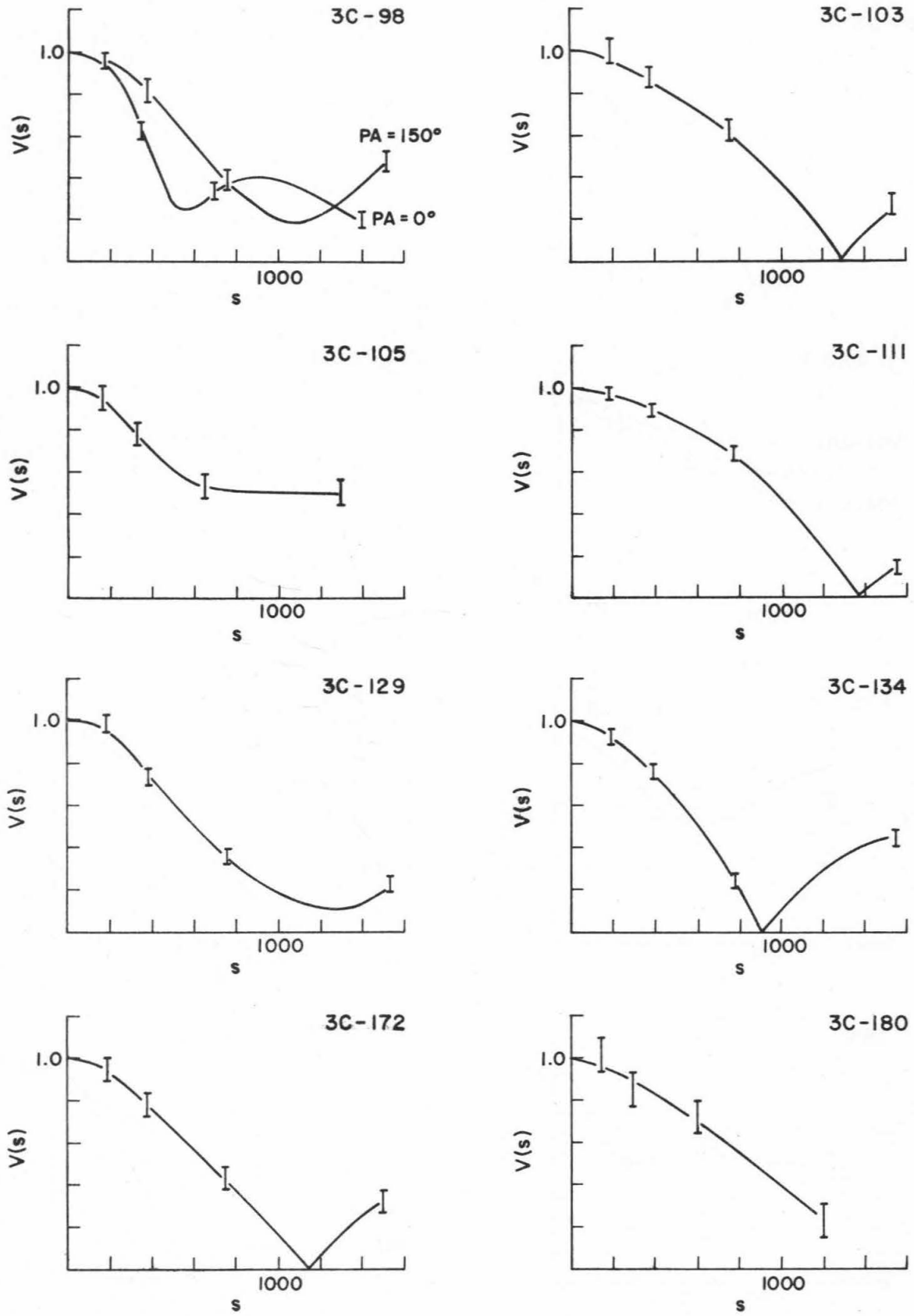
3C-98
1.0
V(s)
PA = 150°
PA = 0°
1000
s
3C-103
1.0
V(s)
1000
s
3C-105
1.0
V(s)
1000
s
3C-111
1.0
V(s)
1000
s
3C-129
1.0
V(s)
1000
s
3C-134
1.0
V(s)
1000
s
3C-172
1.0
V(s)
1000
s
3C-180
1.0
V(s)
1000
s

FIGURE 3

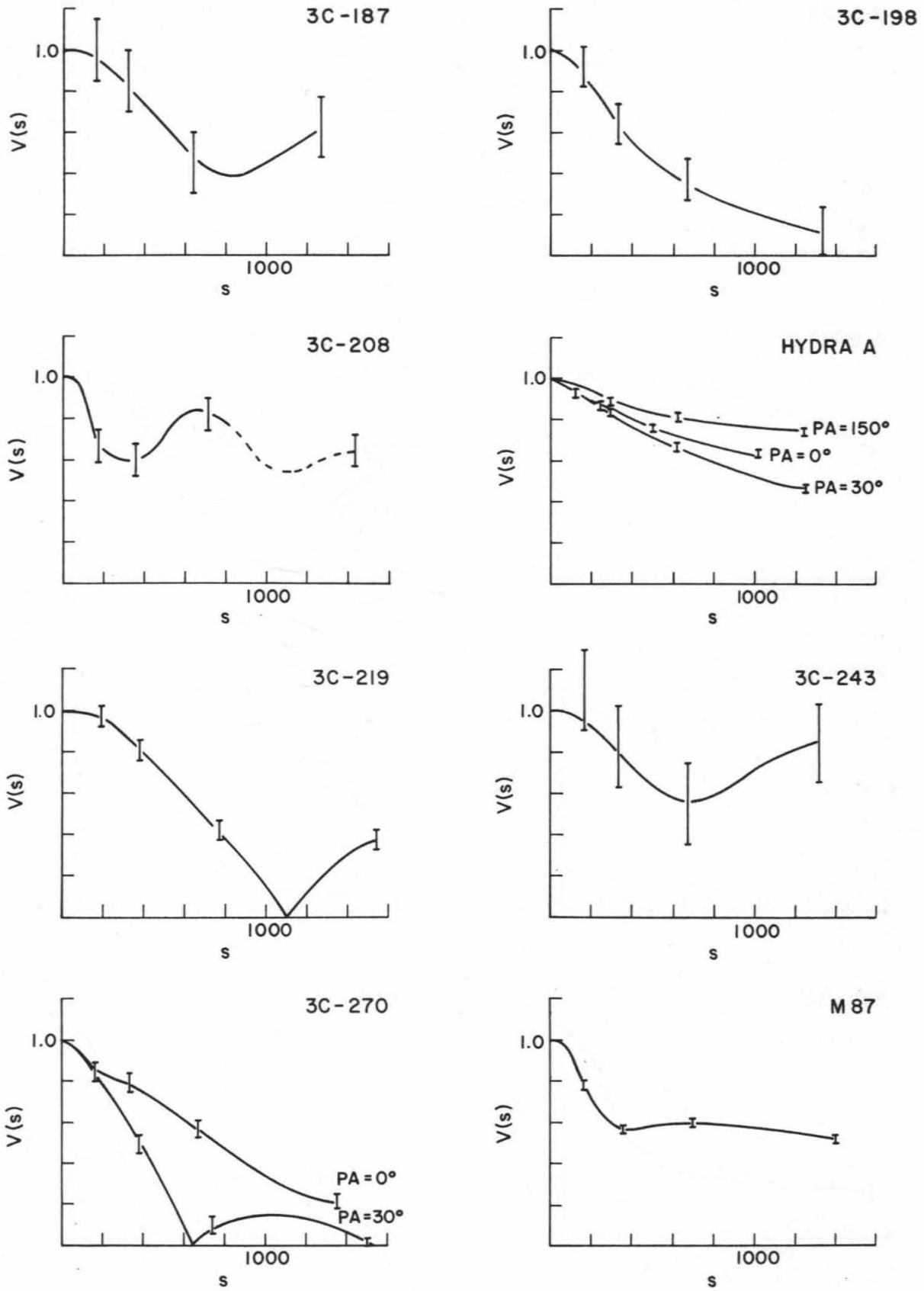
3C-187
3C-198
3C-208
HYDRA A
PA=150°
PA=0°
PA=30°
3C-219
3C-243
3C-270
PA=0°
PA=30°
M 87
1.0
V(s)
1000
s

FIGURE 4

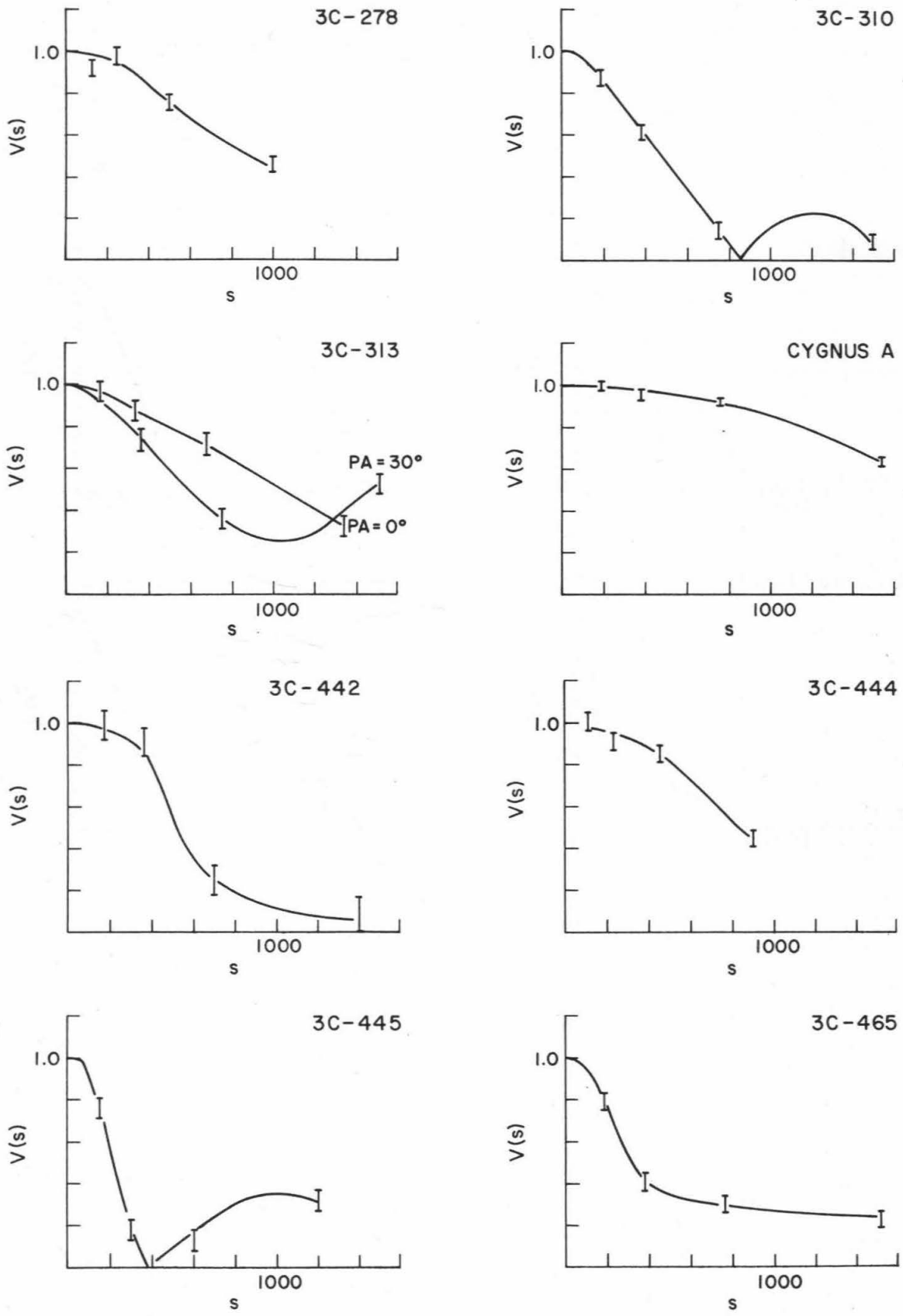
3C-278
1.0
V(s)
1000
s
3C-310
1.0
V(s)
1000
s
3C-313
1.0
V(s)
PA = 30°
PA = 0°
1000
s
CYGNUS A
1.0
V(s)
1000
s
3C-442
1.0
V(s)
1000
s
3C-444
1.0
V(s)
1000
s
3C-445
1.0
V(s)
1000
s
3C-465
1.0
V(s)
1000
s

FIGURE 5

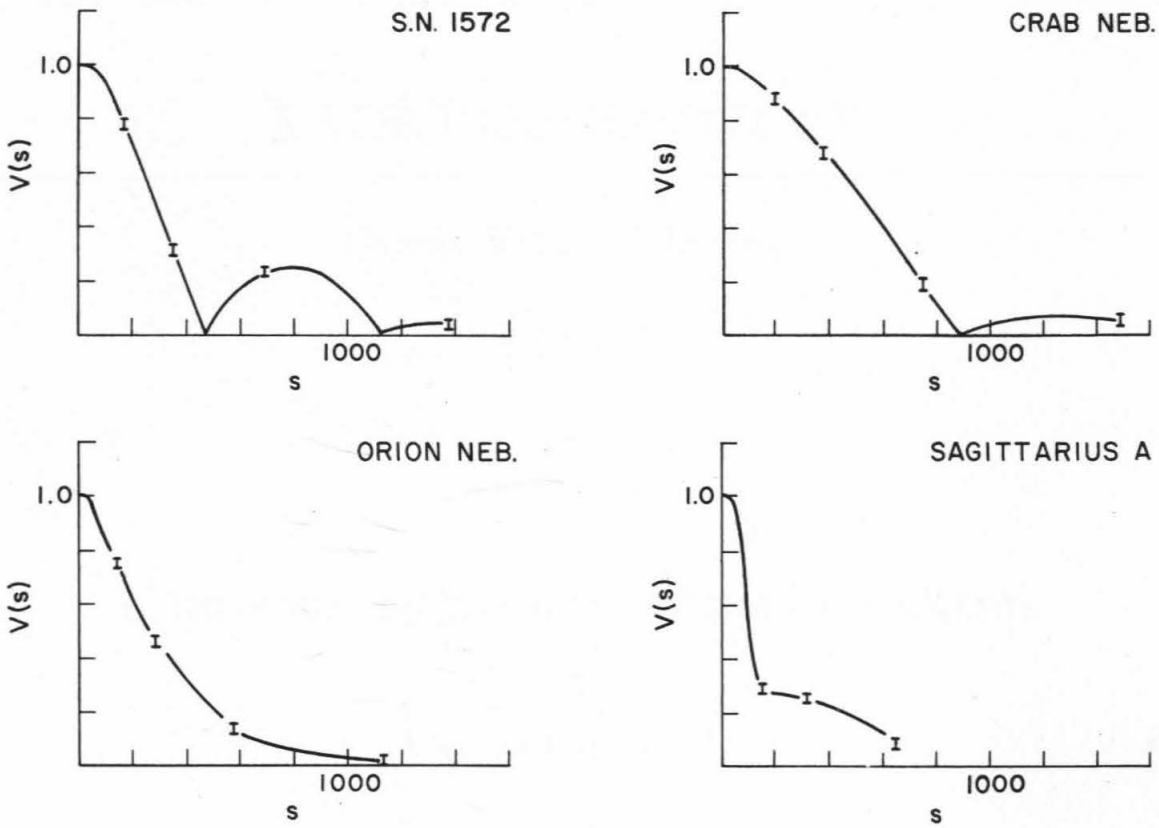

FIGURE 6